

# MIXED PRECISION AND MIXED ACCURACY EXPLICIT TWO-DERIVATIVE RUNGE-KUTTA METHODS

SIGAL GOTTLIEB, ZACHARY J. GRANT, AND CÉSAR HERRERA

**ABSTRACT.** Mixed precision Runge–Kutta methods have been recently developed and used for the time-evolution of partial differential equations. Two-derivative Runge–Kutta schemes may offer enhanced stability and accuracy properties compared to classical one-derivative methods, making them attractive in a wide variety of problems. However, their computational cost can be significant, motivating the use of a mixed-precision paradigm that employs different floating-point precisions for different function evaluations to balance efficiency and accuracy. To ensure that the perturbations introduced by the low precision computations do not destroy the accuracy of the solution, we need to understand how these perturbation errors propagate. We extend the numerical analysis mixed precision framework previously developed for Runge–Kutta methods to characterize the propagation of the perturbation errors arising from mixed precision computations in explicit and implicit two-derivative Runge–Kutta methods. We use this framework for analyzing the order of the perturbation errors, and for designing new methods that are less sensitive to the effect of the low precision computations. Numerical experiments on linear and nonlinear representative PDEs, demonstrate that appropriately designed mixed-precision two-derivative Runge–Kutta methods achieve the predicted accuracy.

## 1. OVERVIEW

In numerically solving a partial differential (PDE) equation of the form

$$(1.1) \quad U_t = f(U, U_x, U_{xx}),$$

we often adopt a method of lines (MOL) approach where the spatial derivatives on the right hand side are first approximated by some numerical approach (e.g. finite differences, finite elements, spectral methods), to obtain

---

This material is based upon work supported by the National Science Foundation under Grant No. DMS-1929284 while the three authors were in residence at the Institute for Computational and Experimental Research in Mathematics in Providence, RI, during the “Empowering a Diverse Computational Mathematics Research Community” program. SG’s research was supported in part by AFOSR Grant No. FA9550-23-1-0037, DOE Grant No. DE-SC0023164 Subaward RC114586, and Mass Dartmouth’s Marine and Undersea Technology (MUST) Research Program funded by the ONR Grant No. N00014-20-1-2849. ZJG’s research was supported in part by DOE grant No. DE-SC0023164 Subaward RC114586 and AFOSR Grant No. FA9550-23-1-0037.

the semi-discretized system of equations

$$(1.2) \quad u_t = F(u),$$

(where  $u$  is a vector of approximations to  $U$ ). This system can then be evolved forward using a high order time stepping method, for example a Runge–Kutta method,

$$(1.3a) \quad y^{(i)} = y_n + \Delta t \sum_{j=1}^s a_{ij} F(y^{(j)})$$

$$(1.3b) \quad y_{n+1} = y_n + \Delta t \sum_{i=1}^s b_i F(y^{(i)}).$$

or a Taylor-series (multiderivative) method,

$$(1.4) \quad y_{n+1} = y_n + \sum_{i=1}^{\ell} b_i \Delta t^i \frac{d^i F}{dy^i}(y_n).$$

In this work we focus on a combination of these approaches: multi-stage multi-derivative methods. In particular, we explore two-derivative Runge–Kutta methods.

The idea of enhancing Runge–Kutta methods with additional derivatives was proposed in the 1950s and 1960s in [31, 30], and multistage multi-derivative time integrators for ordinary differential equations were studied in [27, 28, 15, 16, 22, 24, 6]. More recently, two-derivative Runge–Kutta methods were applied to the time evolution of PDEs [9, 1, 18, 25, 10]. In this work we consider two-derivative Runge–Kutta methods for the time-evolution of PDEs of the form (1.1), combining this approach with mixed precision computation meant to improve efficiency while retaining accuracy.

Modern computing architectures have resulted in recent emphasis on mixed precision computations. This is because the dominant cost is no longer the computational arithmetic (measured in FLOPS), but other factors such as memory bandwidth, data movement, and energy consumption. Lower precision is often advantageous because it significantly reduces these computational costs. However, higher precision is often necessary to obtain stable and accurate simulations. Mixed precision approaches have become very popular in numerical linear algebra [21, 5, 19]. More recently, mixed precision approaches for the numerical solution of time-dependent PDEs have been proposed and shown to be accurate and efficient [12, 8, 2, 20, 26, 4, 3]. These approaches use lower precision when possible, and combine them with higher precision when needed. The ideal scenario is a combination of the efficiency of low precision and the accuracy of high precision that allows us to enjoy the best of both worlds. In this work we extend the numerical analysis framework for mixed precision Runge–Kutta methods introduced in [12] to mixed precision two-derivative Runge–Kutta methods. This approach allows us to understand the effect of

the perturbation errors induced by the low precision computations, and to design methods that mitigate their impact on the overall solution.

We note that although our primary motivation is mixed precision simulations, this framework applies to a variety of other scenarios. Whenever a part of the simulation is computed with less accuracy, the framework we describe in Section 4 can be adapted to understand the propagation of the errors. This framework explains the overall impact of computing only the second order derivative with less accuracy. In fact, in many mixed accuracy methodologies the framework we describe in Section 4 simplifies due to the smoothness of the perturbation introduced, which allows cancellation errors which cannot be relied upon when the perturbation is non-smooth, such as in the mixed precision case.

The structure of the paper is as follows: in Section 2 we review the current state of mixed precision methods for the numerical solution of time-dependent PDEs. In Section 2.1 we discuss the theoretical framework introduced in [12] for mixed precision Runge–Kutta methods. In Section 2.2 we briefly discuss the mixed precision techniques in exponential time integration methods introduced in [2], and in Section 2.3 the mixed precision Runge–Kutta–Chebyshev methods of [8]. In Subsection 2.4 we review the mixed precision WENO finite difference method introduced in [26]. In Section 3 we present two-derivative methods and their recent use in hyperbolic PDEs.

In Section 4 we present the mixed precision two-derivative Runge–Kutta framework, following the approach in [12]. We use a simplified framework that assumes that only computations of the second derivative are performed in low precision, and use this framework to establish order conditions for the low precision perturbation. In Section 5 we present third, fourth, fifth, and sixth order mixed precision methods with various perturbation orders. In Section 6 we present the mixed precision numerical simulations that show that the numerical results are as predicted by the theory. Finally, in Section 7 we present our conclusions and discuss possible future directions of this approach.

## 2. BACKGROUND: MIXED PRECISION METHODS FOR PDEs

The use of mixed precision for the solution of PDEs is relatively new. In this section we review the existing work on mixed precision methods used in the context of PDEs.

**2.1. Mixed Precision Runge–Kutta methods.** A mixed accuracy framework for Runge–Kutta methods was introduced in [12] with an emphasis on designing mixed-precision implicit Runge–Kutta methods. This work utilizes lower-precision arithmetic in the implicit computation of a multi-stage time integrator without destroying the overall accuracy of the solution. The mechanism behind this approach takes advantage of the multi-stage nature of the scheme to damp out the errors from the low-precision computation.

The key idea is that the implicit solves (or the expensive part of the implicit solve) can be evaluated in low precision such as half (**Float16**) or single (**Float32**) precision, while the explicit computations are computed in high precision, leading to a highly accurate final update.

As a simple example, consider the diagonally implicit Runge–Kutta method

$$(2.1a) \quad y^{(i)} = y_n + \Delta t \sum_{j=1}^i a_{ij} F(y^{(j)})$$

$$(2.1b) \quad y_{n+1} = y_n + \Delta t \sum_{i=1}^s b_i F(y^{(i)}),$$

where each stage is computed implicitly, and the final reconstruction is explicit. To make the implicit stages  $y^{(i)}$  cheaper to invert, we replace  $F(y^{(i)})$  with a lower precision function  $F_\varepsilon(y^{(i)})$ . This is harmonious with the numerical linear algebra approaches that iteratively solve the nonlinear system using a mixture of precisions [17]. The mixed precision method then becomes:

$$(2.2a) \quad y^{(i)} = y_n + \Delta t \left( \sum_{j=1}^{i-1} a_{ij} F(y^{(j)}) + a_{ii} F_\varepsilon(y^{(i)}) \right)$$

$$(2.2b) \quad y_{n+1} = y_n + \Delta t \sum_{i=1}^s b_i F(y^{(i)}).$$

This strategy introduces a perturbation into the internal stages. The key to mixed precision methods is that this perturbation must be controlled by computing (and when needed re-computing) the function evaluations in high precision so that the overall solution is minimally impacted by it.

Grant [12] introduced a general theoretical additive perturbation framework showing how perturbations from low precision can be controlled. Within this framework, specific order conditions are derived that track the propagation of the perturbation errors introduced by the lower precision computations, and enable the characterization of which operations may be safely computed in lower precision.

The mixed precision implementation of the fully implicit Runge–Kutta method (1.3) can be re-written as

$$(2.3a) \quad \mathbf{y} = u^n \mathbf{e} + \Delta t \tilde{\mathbf{A}}_{ij} F(\mathbf{y}) + \varepsilon \Delta t \mathbf{A}_\varepsilon \tau(\mathbf{y})$$

$$(2.3b) \quad u^{n+1} = u^n + \Delta t \tilde{\mathbf{b}}_j F(\mathbf{y}) + \varepsilon \Delta t \mathbf{b}_\varepsilon \tau(\mathbf{y})$$

where  $\tilde{\mathbf{A}} = \mathbf{A} + \mathbf{A}_\varepsilon$  and  $\tilde{\mathbf{b}} = \mathbf{b} + \mathbf{b}_\varepsilon$ , and

$$\tau(y) = \frac{1}{\varepsilon} (F(y) - F_\varepsilon(y)).$$

Analyzing the scheme in this form allows us to use an additive B-series representation to track the evolution of  $u$  as well as its interaction with the

perturbation function  $\tau$ . For example, a second order expansion is:

$$\begin{aligned} u^{n+1} &= u^n + \Delta t \tilde{\mathbf{b}} F(\mathbf{y}) + \varepsilon \Delta t \mathbf{b}_\varepsilon \tau(\mathbf{y}) \\ &= u^n + \Delta t \tilde{\mathbf{b}} F \left( u^n \mathbf{e} + \Delta t \tilde{\mathbf{A}} F(\mathbf{y}) + \varepsilon \Delta t \mathbf{A}_\varepsilon \tau(\mathbf{y}) \right) + \varepsilon \Delta t \mathbf{b}_\varepsilon \tau(\mathbf{y}) \\ &= u^n + \Delta t \tilde{\mathbf{b}} F(u^n \mathbf{e}) + \Delta t^2 \tilde{\mathbf{b}} \tilde{\mathbf{A}} F_y(u^n) F(\mathbf{y}) + \varepsilon \Delta t^2 \tilde{\mathbf{b}} \mathbf{A}_\varepsilon F_y(u^n) \tau(\mathbf{y}) \\ &\quad + \varepsilon \Delta t \mathbf{b}_\varepsilon \tau(\mathbf{y}) + O(\Delta t^3) + O(\varepsilon \Delta t^3) \end{aligned}$$

so that

$$\begin{aligned} (2.4) \quad u^{n+1} &= \underbrace{u^n + \Delta t \tilde{\mathbf{b}} \mathbf{e} F(u^n) + \Delta t^2 \tilde{\mathbf{b}} \tilde{\mathbf{c}} F_y(u^n) F(u^n)}_{\text{scheme}} \\ &\quad + \underbrace{\varepsilon \left( \Delta t \mathbf{b}_\varepsilon + \Delta t^2 F_y(u^n) \tilde{\mathbf{b}} \mathbf{A}_\varepsilon \right) \tau(\mathbf{y})}_{\text{perturbation}} + O(\Delta t^3) + O(\varepsilon \Delta t^3). \end{aligned}$$

This expansion shows two sources of error: those of the scheme and those of the perturbation.

In the case of a smooth perturbation, we can rely on cancellations, and even expand the  $\tau$  term, and obtain more relaxed conditions. However, in the case where the perturbation is non-smooth, such as mixed precision, we cannot rely on cancellations, or expand the  $\tau$  terms. In this case, if we wish to eliminate the  $\varepsilon \Delta t$  term, it is not enough to require that  $\mathbf{b}_\varepsilon \mathbf{e} = 0$ , rather we require that each element of  $\mathbf{b}_\varepsilon$  is zero.

We can easily extend (2.4) to higher order using the additive B-series analysis of the scheme. The perturbation errors feature a combination of the scheme coefficients and the perturbation coefficients. Expanding the terms to third order in  $\Delta t$  and first order in  $\varepsilon$  we obtain:

Terms involving $\varepsilon$ and $\Delta t$	Terms involving $F$ and $\tau$	scheme coefficients
$\varepsilon \Delta t$	$\tau(u^n)$	$\mathbf{b}_\varepsilon \mathbf{e}$
$\varepsilon \Delta t^2$	$F_y(u^n) \tau(\cdot)$	$\tilde{\mathbf{b}} \mathbf{A}_\varepsilon \mathbf{e}$
$\varepsilon \Delta t^3$	$F_y(u^n) F_y(u^n) \tau(\cdot)$	$\tilde{\mathbf{b}} \tilde{\mathbf{A}} \mathbf{A}_\varepsilon \mathbf{e}$
$\varepsilon \Delta t^3$	$F_{yy}(u^n) (F(u^n), \tau(\cdot))$	$\tilde{\mathbf{b}} (\tilde{\mathbf{c}} \cdot \mathbf{A}_\varepsilon \mathbf{e})$

From these terms, the consistency conditions for the scheme and the perturbation conditions can be easily defined, even if the perturbation  $\tau$  is poorly behaved, as is expected in mixed precision. For a scheme to achieve order  $O(\varepsilon \Delta t^{m+1})$  we require :

$$m \geq 1 \quad |\mathbf{b}_\varepsilon| \mathbf{e} = 0$$

$$m \geq 2 \quad |\tilde{\mathbf{b}}| |\mathbf{A}_\varepsilon| \mathbf{e} = 0$$

$$m \geq 3 \quad |\tilde{\mathbf{b}}| |\mathbf{A}_\varepsilon| |\tilde{\mathbf{A}}| \mathbf{e} = 0, \quad |\tilde{\mathbf{b}}| |\tilde{\mathbf{A}}| |\mathbf{A}_\varepsilon| \mathbf{e} = 0.$$

We observe that we must have each element of  $\mathbf{b}_\varepsilon$  be zero, and the other conditions depend on which stages are excluded from the final row reconstruction.

Grant's order conditions in [12] show how to design a method to ensure that the low-precision perturbation does not ruin the accuracy of the method. In the simplest and most intuitive sense, we see that a diagonally implicit method of the form (2.2) above introduces the perturbation into the implicit stage only, so that each stage has a perturbation error of  $\Delta t \varepsilon$ , and this is further mitigated at the final stage by another  $\Delta t$ , so that at each step we have a perturbation error of  $\Delta t^2 \varepsilon$ . Growing to a final time of  $T_f$ , we expect  $O(\frac{1}{\Delta t})$  steps and so a final perturbation error of  $\Delta t \varepsilon$ . Explicit [12, 3] or inexpensive implicit [14] corrections can then be used further to improve the perturbation error.

Performance analysis of methods developed or analyzed by the framework introduced in [12] was performed in [4, 3] for small problems, and in [23] on larger ODEs where the implicit problem is solved in low and mixed precision. In [13] the methods of [12] were tested with state-of-the-art software using the Ginkgo library.

**Remark 2.1.** *We note that while mixed precision has only recently been used in this context, the implicit stages are rarely computed exactly and some perturbation is introduced whenever the implicit stage is approximated by some iterative procedure such as Newton's iteration. For this reason, perturbation analysis is always important for implicit methods; however, the perturbations introduced by mixed precision are non-smooth, and so more difficult to handle. The mixed precision order conditions introduced in [12] allow us to deal with any type of perturbation, whether smooth (such as linearization) or non-smooth (such as rounding error in low precision).*

**2.2. Mixed precision exponential time stepping methods.** Mixed precision approaches have been most heavily developed in the context of numerical linear algebra methods. It is natural, then, that numerical methods for time-evolution that have the closest relationship to numerical linear algebra will take advantage of the mixed precision paradigm. In [2], the mixed precision paradigm was leveraged for efficiency in solving an advection-diffusion-reaction PDE using exponential time integration methods. Two approaches were studied in conjunction with exponential time integrators. First, the authors reformulated the exponential Rosenbrock-Euler method in a way that allows for low precision computations of the matrix exponential which improves efficiency while improving accuracy over the low precision version. Next, the authors use a mixed precision Krylov approach for computing matrix exponentials, which was more efficient than the full precision approach and more accurate than the low precision approach.

**2.3. Mixed precision explicit Runge–Kutta–Chebyshev methods.** While the methods developed [12] and the follow-up work in [4, 3, 13, 23] focused on implicit Runge–Kutta methods, where the expensive implicit solves dominate runtime, this is not the only avenue in which mixed precision

has significant potential to accelerate computations without significantly degrading accuracy.

When dealing with “stiff” differential equations, where the eigenvalues are on the negative real axis, the solution decays rapidly, necessitating a careful choice of the numerical method. Typically, explicit methods are inexpensive but require very small time-steps when solving the such equations. However, Runge–Kutta–Chebyshev methods are explicit first and second order Runge–Kutta type methods with a large number of stages  $s$ , that feature very large linear stability regions along the negative real axis. Just like the Gauss–Chebyshev–Lobatto quadrature methods, these Runge–Kutta methods use the recurrence relation definition of the Chebyshev polynomial to create a low storage formula that results in a second order approximation to the solution of an ODE system. If a large linear negative-real-axis stability region is desired, this method may have a very large number of stages  $s$ . Furthermore, this method is built recursively at each time-step. These two factors make these explicit Runge–Kutta methods computationally costly.

However, since the polynomial is built recursively, one can achieve high order accuracy by computing most of the stages in low precision, with only a few stages computed in high precision. Using this insight, Croci & de Souza [8] suggested a mixed precision approach that exploits a clever re-writing of these methods to allow for an inexpensive mixed precision implementation to design explicit Runge–Kutta Chebyshev methods with a mixed precision paradigm. This work showed that while careless use of low precision may break convergence, carefully chosen high-precision function evaluations allow for order-preserving mixed precision that is computationally efficient.

**2.4. Mixed Precision WENO.** Another notable use of mixed precision in time-dependent simulation of a hyperbolic problem was in [26], where a novel mixed-precision weighted essentially non-oscillatory (WENO) method was developed and used for solving the Teukolsky equation. This hyperbolic PDE arises when modeling perturbations of Kerr black holes. In these simulations, we require very long-time evolution, in which rounding error may build up. For this reason, high order discretizations and quad precision (Float128) are needed to accurately evolve the solution. In [26], the authors showed that while quad precision simulation is needed for the long time evolution, not all parts of the WENO algorithm need be performed in quad precision. In particular, the expensive nonlinear computation of the WENO weights was performed in reduced precision, while requiring that the WENO weights sum to one in quad precision. The optimized and accelerated WENO code took seven days to run in quad precision. The mixed precision implementation took only two days to run, a significant speedup factor of 3.3x, while producing equally accurate results.

### 3. BACKGROUND: TWO DERIVATIVE RUNGE–KUTTA METHODS

Two derivative Runge–Kutta (TDRK) methods were applied to the time evolution of PDEs in [9, 1, 18, 25, 10]. When applied to a system of ODEs (1.2) resulting from a semi-discretization of a PDE (1.1), a TDRK can be written as:

$$(3.1) \quad \begin{aligned} y^{(i)} &= u^n + \Delta t \sum_{j=1}^s a_{ij} F(y^{(j)}) + \Delta t^2 \sum_{j=1}^s \dot{a}_{ij} \dot{F}(y^{(j)}), \quad i = 1, \dots, s \\ u^{n+1} &= u^n + \Delta t \sum_{j=1}^s b_j F(y^{(j)}) + \Delta t^2 \sum_{j=1}^s \dot{b}_j \dot{F}(y^{(j)}), \end{aligned}$$

or, in matrix form

$$(3.2) \quad \begin{aligned} \mathbf{y} &= u^n + \Delta t \mathbf{A} F(\mathbf{y}) + \Delta t^2 \dot{\mathbf{A}} \dot{F}(\mathbf{y}) \\ u^{n+1} &= u^n + \Delta t \mathbf{b} F(\mathbf{y}) + \Delta t^2 \dot{\mathbf{b}} \dot{F}(\mathbf{y}) \end{aligned}$$

where  $\mathbf{A}_{ij} = a_{ij}$ ,  $\dot{\mathbf{A}} = \dot{a}_{ij}$ , and  $\mathbf{b}$  and  $\dot{\mathbf{b}}$  are vectors with the elements  $b_j$  and  $\dot{b}_j$ , respectively. The order conditions for this method up to sixth order are in given in Appendix A of [11]. In this work we wish to focus only on explicit methods, so that the sums at the  $i$ th stage of (3.1) go up to  $i - 1$  rather than  $s$ , and correspondingly the matrices  $\mathbf{A}$  and  $\dot{\mathbf{A}}$  are strictly lower triangular.

We note that in Tsai’s work [6] a simplified (and less general) version of these methods is given in the form

$$(3.3) \quad \begin{aligned} y^{(1)} &= u^n \\ y^{(i)} &= u^n + \Delta t a_{i1} F(y^{(1)}) + \Delta t^2 \sum_{j=1}^{i-1} \dot{a}_{ij} \dot{F}(y^{(j)}), \quad i = 2, \dots, s \\ (3.4) \quad u^{n+1} &= u^n + \Delta t F(y^{(1)}) + \Delta t^2 \sum_{j=1}^s \dot{b}_j \dot{F}(y^{(j)}). \end{aligned}$$

An advantage of this form is the simplified order conditions. In some cases this form may also be advantageous for mixed precision purposes.

TDRKs are especially appealing when dealing with hyperbolic conservation laws of the form

$$(3.5) \quad U_t + f(U)_x = 0,$$

where the computation of  $f'(U)$  is generally needed for flux splitting in the spatial discretization. The second derivative computation  $\dot{F}$  can re-use the computation of this Jacobian, which makes the TDRK methods natural in this context.

Consider the spatial discretization of (3.5), where the method-of-lines approach leads to the system

$$u_t = -\mathbf{D}_x f(u) = F(u),$$

for some differentiation matrix  $\mathbf{D}_x$ . The computation of the second derivative term  $\dot{F}$  follows directly from the definition of  $F$ ,

$$\dot{F} = F(u)_t = F_u u_t = F_u F.$$

In practice [7] we can use a Lax-Wendroff type approach to compute  $U_{tt} \approx \dot{F}$ :

$$U_{tt} = -f(U)_{xt} = -(-f'(U)f(U)_x)_x,$$

so that

$$\dot{F}(u) \approx -\mathbf{D}_x (f'(u)F(u)),$$

where  $f'(u)$  is pre-computed for the flux splitting. In the next section we develop a mixed precision framework for TDRK methods.

#### 4. A MIXED PRECISION FRAMEWORK FOR TWO-DERIVATIVE RUNGE-KUTTA METHODS

We consider a mixed precision approach to the two-derivative Runge-Kutta method (3.1). In principal, we can consider either  $F$  or  $\dot{F}$  (or both) to be in low precision, but we currently focus on the case where the computation of the second derivative is performed in low precision, due to the fact that this term enters with a  $\Delta t^2$  multiplication which naturally reduces the impact of the low-precision perturbation. A more general approach is possible, and may be explored in future work.

The low-precision computation of the second derivative is particularly advantageous where this term is costly to compute and we wish to compute it in a cheaper, albeit less accurate, way. We focus on the mixed precision form

$$(4.1) \quad \begin{aligned} y^{(i)} &= u^n + \Delta t \sum_{j=1}^s a_{ij} F(y^{(j)}) + \Delta t^2 \sum_{j=1}^s \dot{a}_{ij} \dot{F}_\varepsilon(y^{(j)}), \quad i = 1, \dots, s \\ u^{n+1} &= u^n + \Delta t \sum_{j=1}^s b_j F(y^{(j)}) + \Delta t^2 \sum_{j=1}^s \dot{b}_j \dot{F}_\varepsilon(y^{(j)}), \end{aligned}$$

where  $\dot{F}_\varepsilon$  denotes the low precision computation of the second derivative  $\dot{F}$ . In matrix form, this becomes

$$(4.2) \quad \begin{aligned} \mathbf{y} &= u^n + \Delta t \mathbf{A} F(\mathbf{y}) + \Delta t^2 \dot{\mathbf{A}}_\varepsilon \dot{F}_\varepsilon(\mathbf{y}) \\ u^{n+1} &= u^n + \Delta t \mathbf{b} F(\mathbf{y}) + \Delta t^2 \dot{\mathbf{b}}_\varepsilon \dot{F}_\varepsilon(\mathbf{y}), \end{aligned}$$

Where the coefficients  $\dot{\mathbf{A}}$  and  $\dot{\mathbf{b}}$  in (3.2) are replaced by  $\dot{\mathbf{A}}_\varepsilon$  and  $\dot{\mathbf{b}}_\varepsilon$  to emphasize that they correspond to low precision computations.

We extend the mixed precision framework in [12] to (4.2), first by re-writing the method in the perturbed form. To distinguish between the behavior of the derivative which should contribute to the accuracy, and the behavior of the perturbation, which we wish to eliminate when possible, we use the notation

$$\dot{F}_\varepsilon = \dot{F} + \varepsilon \dot{\tau}$$

where  $\dot{\tau}$  is *not* the derivative of the perturbation  $\tau$ , but a perturbation of the derivative  $\dot{F}$ . Plugging this into (4.2) we obtain

$$(4.3) \quad \begin{aligned} \mathbf{y} &= u^n + \Delta t \mathbf{A} F(\mathbf{y}) + \Delta t^2 \dot{\mathbf{A}} \dot{F}(\mathbf{y}) + \varepsilon \Delta t^2 \dot{\mathbf{A}}_\varepsilon \dot{\tau} \\ u^{n+1} &= u^n + \Delta t \mathbf{b} F(\mathbf{y}) + \Delta t^2 \dot{\mathbf{b}} \dot{F} + \varepsilon \Delta t^2 \dot{\mathbf{b}}_\varepsilon \dot{\tau}, \end{aligned}$$

where for clarity we use the coefficients  $\dot{\mathbf{A}}$  and  $\dot{\mathbf{b}}$  attached to  $\dot{F}$  and the coefficients  $\dot{\mathbf{A}}_\varepsilon$   $\dot{\mathbf{b}}_\varepsilon$  attached to  $\dot{\tau}$ , even though in our case  $\dot{\mathbf{A}} = \dot{\mathbf{A}}_\varepsilon$  and  $\dot{\mathbf{b}} = \dot{\mathbf{b}}_\varepsilon$ .

We can Taylor expand this form to obtain the following terms, and match them to the desired order:

$$\begin{aligned} O(\Delta t): \quad \mathbf{b}\mathbf{e} &= 1 \\ O(\Delta t^2): \quad \mathbf{b}\mathbf{c} + \dot{\mathbf{b}}\mathbf{e} &= \frac{1}{2} & O(\varepsilon \Delta t^2): \quad \left| \dot{\mathbf{b}}_\varepsilon \right| \mathbf{e} &= 0 \\ O(\Delta t^3): \quad \mathbf{b}\mathbf{A}\mathbf{c} + \mathbf{b}\dot{\mathbf{A}}\mathbf{e} + \dot{\mathbf{b}}\mathbf{c} &= \frac{1}{6} & O(\varepsilon \Delta t^3): \quad \left| \mathbf{b} \right| \left| \dot{\mathbf{A}}_\varepsilon \right| \mathbf{e} &= 0 \\ O(\Delta t^3): \quad \mathbf{b}\mathbf{c}^2 + 2\dot{\mathbf{b}}\mathbf{c} &= \frac{1}{3} & O(\varepsilon \Delta t^3): \quad \left| \dot{\mathbf{b}}_\varepsilon \right| \left| \mathbf{c} \right| &= 0 \end{aligned}$$

where  $\mathbf{c}^2$  is understood as element-wise squaring, and the absolute value  $|\cdot|$  is understood element-wise both for matrices and vectors. In this work we limit the perturbation conditions to third order. Expanding to higher order terms will produce more order and perturbation conditions.

**First order perturbation error:** All methods that satisfy the formulation (4.2) where all the evaluations of  $F$  are in full precision, have the property that the perturbation enters as  $\varepsilon \Delta t^2$  at each time-step. Once again, evolving to a final time requires  $O(\frac{1}{\Delta t})$  steps, so that the perturbation error builds up to  $E_{pert} = O(\varepsilon \Delta t)$ . Thus, all methods of the form (4.2) have overall final-time error

$$E = E_{method} + E_{pert} = O(\Delta t^p) + O(\varepsilon \Delta t).$$

We expect to see an order of  $p$  as long if  $\varepsilon \ll \Delta t^{p-1}$ , and first order as  $\Delta t$  gets smaller.

**Second order perturbation error:** To improve the errors resulting from the low precision perturbation, we can design a TDRK method so that the perturbation condition corresponding to  $\varepsilon \Delta t^2$  is satisfied:

$$(4.4) \quad \left| \dot{\mathbf{b}}_\varepsilon \right| \mathbf{e} = 0, \rightarrow \left( \dot{\mathbf{b}}_\varepsilon \right)_j = 0, \quad \forall j.$$

This condition means that the second derivative terms computed in low precision do not enter in the reconstruction stage. A method of the form (4.2) that additionally satisfies this perturbation condition, will have final time-error

$$E = E_{method} + E_{pert} = O(\Delta t^p) + O(\varepsilon \Delta t^2).$$

We expect to see order  $p$  convergence if  $\varepsilon \ll \Delta t^{p-2}$ , and second order for the regime where  $\Delta t$  gets smaller.

**Third order perturbation error:** Continuing with this approach, we can zero out the perturbation errors that correspond the  $\varepsilon\Delta t^3$ , by additionally requiring  $|\dot{\mathbf{b}}_\varepsilon| |\mathbf{A}| \mathbf{e} = 0$  and  $|\mathbf{b}| |\dot{\mathbf{A}}_\varepsilon| \mathbf{e} = 0$ . The first of these conditions is automatically satisfied by  $(\dot{\mathbf{b}}_\varepsilon)_j = 0, \forall j$ , so we need only impose

$$(4.5) \quad \sum_{i=1}^s |b_i| \sum_{j=1}^s \left| (\dot{\mathbf{A}}_\varepsilon)_{ij} \right| = 0.$$

This condition ensures that the method does not include in the final reconstruction any stage that has a perturbed value, which gives us a perturbation error of  $O(\varepsilon\Delta t^4)$ . At the final time we expect an error of

$$E = E_{method} + E_{pert} = O(\Delta t^p) + O(\varepsilon\Delta t^3).$$

We expect to see an order of  $p$  as long if  $\varepsilon \ll \Delta t^{p-3}$ , and third order as  $\Delta t$  gets smaller.

**Remark 4.1.** *It is important to note that the value of  $\varepsilon$  is not the machine zero associated with the low precision. While  $\varepsilon$  is clearly connected with the number of digits retained in the lower precision, it also depends on the number of computations to evaluate the operator, and how they are performed. For example, if we square a low precision matrix of dimensions  $N_x \times N_x$ , we expect that the  $N_x^2$  multiplications and  $N_x$  additions performed to evaluate each low precision computation would result in a much larger  $\varepsilon$  than one would naively expect from the low precision machine zero! On the other hand, performing this matrix multiplication in high precision and then casting it to lower precision for use at each stage will allow for a smaller  $\varepsilon$ , but would increase the computational cost. We see in the numerical examples below (Figure 6) the impact of the computation of the low precision operator on the value of  $\varepsilon$ .*

## 5. EXPLICIT MIXED PRECISION TDRKs

In this section focus on explicit mixed precision TDRKs. We provide explicit mixed precision methods that have final time errors

$$E = O(\Delta t^p) + O(\varepsilon\Delta t^m)$$

of orders  $p = 3, 4, 5, 6$ , and various perturbation orders  $m$ . In designing the methods we prioritize simple rational coefficients, which are beneficial for implementation in quad precision. We present the linear stability regions of these methods, as well as the impact of a perturbation on these stability regions. In Section 6 we will verify that these methods obtain the design order of accuracy and perturbation.

5.1. **Third order methods.** We begin with a method found in [6]:

**TDRK method TDRK2s3p1e:** The two-stage third order method

$$(5.1) \quad \begin{aligned} y^{(1)} &= u^n + \Delta t F(u^n) + \frac{\Delta t^2}{2} \dot{F}_\varepsilon(u^n) \\ u^{n+1} &= u^n + \Delta t F(u^n) + \frac{\Delta t^2}{6} (2\dot{F}_\varepsilon(u^n) + \dot{F}_\varepsilon(y^{(1)})) \end{aligned}$$

will have final time error

$$E = O(\Delta t^3) + O(\varepsilon \Delta t).$$

This method takes Tsai's form (3.3) so that we only need to compute the high precision value  $F(u^n)$  once per time-step, which also provides computational savings. We can improve the perturbation error by requiring that the final reconstruction does not include any second derivative terms, but then Tsai's form is not possible.

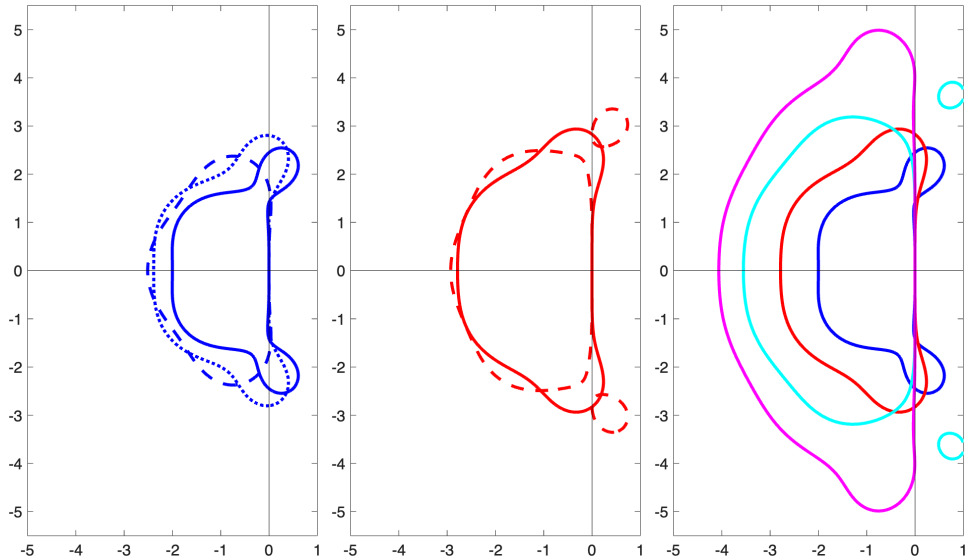


FIGURE 1. Linear stability regions for the MP-TDRK methods with error  $O(\Delta t^p)$  and perturbation error  $O(\varepsilon \Delta t^m)$ . Third order in blue, fourth order in red, fifth order in cyan, sixth order in magenta. Solid lines are perturbation error  $m = 1$ , dashed lines are  $m = 2$ , and dotted line  $m = 3$ . Left: Third order methods. Center: Fourth order methods. Right: All methods with perturbation order  $m = 1$ .

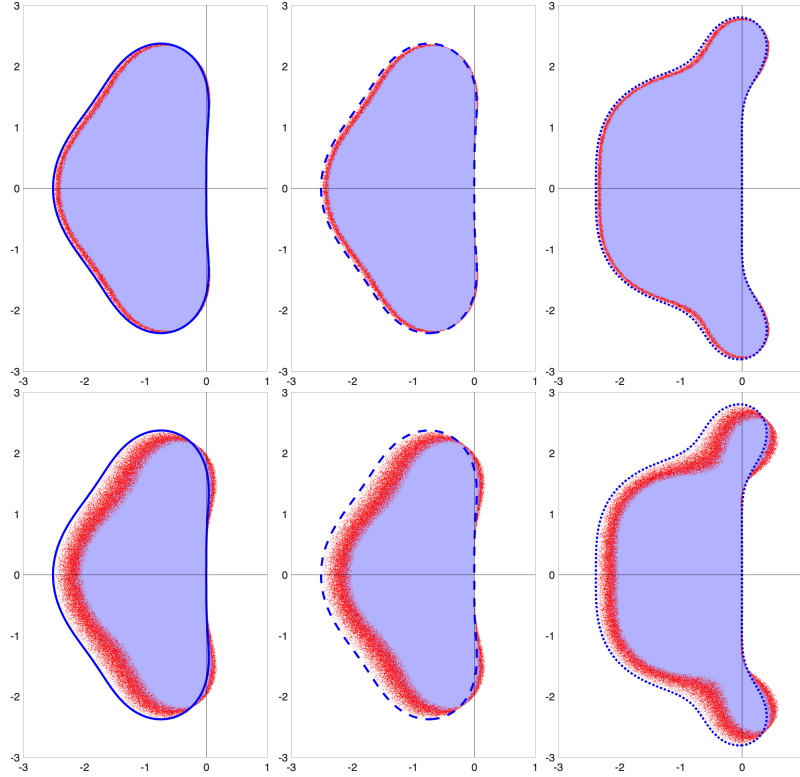


FIGURE 2. Perturbed Linear stability regions for the third order MP-TDRK methods. Top:  $\varepsilon = 0.1$ ; Bottom:  $\varepsilon = 0.5$ . Left: the MP-TDRK2s3p1e method (5.1). Middle: MP-TDRK2s3p2e method (5.2). Right: MP-TDRK3s3p3e method (5.3).

**TDRK method TDRK2s3p2e:** This two-stage third order method satisfies Condition (4.4):

$$\begin{aligned}
 y^{(1)} &= u^n + \frac{2}{3}\Delta t F(u^n) + \frac{2}{9}\Delta t^2 \dot{F}_\varepsilon(u^n) \\
 (5.2) \quad u^{n+1} &= u^n + \frac{1}{4}\Delta t F(u^n) + \frac{3}{4}\Delta t F(y^{(1)})
 \end{aligned}$$

This method will have a final time error of

$$E = O(\Delta t^3) + O(\varepsilon \Delta t^2).$$

Adding the condition (4.5) we obtain a method with higher order  $m$  in the perturbation error:

**TDRK method TDRK3s3p3e:** This three stage third order method

$$(5.3) \quad \begin{aligned} y^{(1)} &= u^n + \frac{2}{3}\Delta t F(u^n) + \frac{2}{9}\Delta t^2 \dot{F}_\varepsilon(u^n) \\ y^{(2)} &= u^n + \frac{1}{3}\Delta t F(u^n) + \frac{1}{3}\Delta t F(y^{(1)}) \\ u^{n+1} &= u^n + \frac{1}{4}\Delta t F(u^n) + \frac{3}{4}\Delta t F(y^{(2)}) \end{aligned}$$

will have a final time error of

$$E = O(\Delta t^3) + O(\varepsilon \Delta t^3).$$

In Figure 1 (left) we plot the linear stability regions of these three third order methods. The stability region of the TDRK2s3p2e method (5.2) is smaller than that of the TDRK2s3p1e method (5.1), but it allows for a higher perturbation order  $m$ . The TDRK3s3p3e method (5.3) requires an additional stage to obtain  $m = 3$ , but this is offset by the larger stability region. We also want to understand the impact of the perturbation error  $\varepsilon$  on the linear stability region of these methods. To emulate this, we incorporate an additional random number of magnitude  $(0, \varepsilon)$  into the second derivative term in the stability polynomial and plot the resulting linear stability regions. These are represented in Figure 2 for  $\varepsilon = 0.1$  and  $\varepsilon = 0.5$ , where  $\varepsilon$  depends upon the precision, the size of the problem, and other implementation-dependent factors. We observe that the larger the perturbation error  $\varepsilon$ , the smaller the linear stability region.

**5.2. Fourth Order Methods.** The unique explicit two stage fourth order TDRK method [6] forms the basis for the first fourth order mixed precision method:

**TDRK method TDRK2s4p1e:** This two-stage fourth order method

$$(5.4) \quad \begin{aligned} y^{(1)} &= u^n + \frac{\Delta t}{2} F(u^n) + \frac{\Delta t^2}{8} \dot{F}_\varepsilon(u^n) \\ u^{n+1} &= u^n + \Delta t F(u^n) + \frac{\Delta t^2}{6} (\dot{F}_\varepsilon(u^n) + 2\dot{F}_\varepsilon(y^{(1)})), \end{aligned}$$

will have a final time error of

$$E = O(\Delta t^4) + O(\varepsilon \Delta t).$$

To obtain  $m = 2$  we require an additional stage to satisfy the additional perturbation conditions (4.4):

**TDRK method TDRK3s4p2e:** The three-stage fourth order method

$$(5.5) \quad \begin{aligned} y^{(1)} &= u^n + \frac{\Delta t}{2} F(u^n) + \frac{\Delta t^2}{8} \dot{F}_\varepsilon(u^n) \\ y^{(2)} &= u^n + \Delta t F(u^n) + \frac{\Delta t^2}{2} \dot{F}_\varepsilon(y^{(1)}) \\ u^{n+1} &= u^n + \frac{1}{6}\Delta t \left( F(u^n) + 4F(y^{(1)}) + F(y^{(2)}) \right), \end{aligned}$$

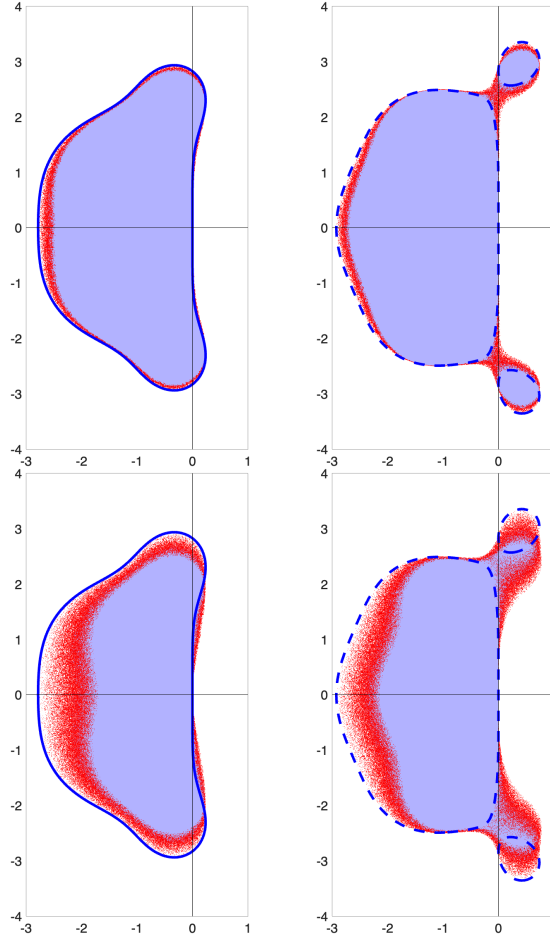


FIGURE 3. Perturbed Linear stability regions for the fourth order MP-TDRK methods. Left: two-stage fourth-order method (5.4). Right: three-stage fourth-order method (5.5). Top:  $\varepsilon = 0.1$ ; Bottom:  $\varepsilon = 0.5$ .

will have a final time error of

$$E = O(\Delta t^4) + O(\varepsilon \Delta t^2).$$

We will need to keep  $\varepsilon \ll \Delta t^2$  to avoid seeing an order reduction to second order. The price we pay is additional function evaluations, which contributes to higher computational cost. Figure 1 (center) shows that there is no significant increase in the size of the stability region to offset this additional cost. Figure 3 shows that the  $m = 1$  TDRK2s4p1e method (5.4) on the left is slightly more impacted by the size of the perturbation than the  $m = 2$  TDRK3s4p2e method (5.5) on the right.

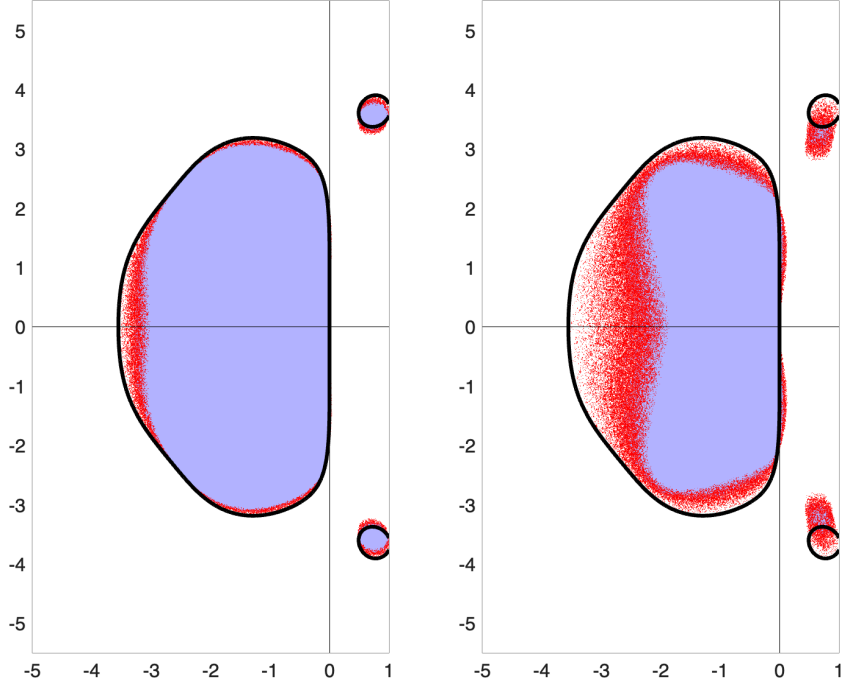


FIGURE 4. Perturbed Linear stability regions for the fifth order MP-TDRK method (5.6) with  $\varepsilon = 0.1$  (left) and  $\varepsilon = 0.5$  (right);

**5.3. Fifth Order Method.** For the fifth order method we use another of Tsai's methods from [6], and implement only the second derivatives in low precision to obtain the mixed precision version.

**TDRK method TDRK3s5p1e:** The three-stage fifth order method

$$\begin{aligned}
 y^{(1)} &= u^n + \frac{1}{3}\Delta t F(u^n) + \frac{1}{18}\Delta t^2 \dot{F}_\varepsilon(u^n) \\
 y^{(2)} &= u^n + \frac{4}{5}\Delta t F(u^n) - \frac{2}{125}\Delta t^2 \dot{F}_\varepsilon(u^n) + \frac{42}{125}\Delta t^2 \dot{F}_\varepsilon(y^{(1)}) \\
 (5.6) \quad u^{n+1} &= u^n + \Delta t F(u^n) + \frac{5}{48}\Delta t^2 \dot{F}_\varepsilon(u^n) + \frac{9}{28}\Delta t^2 \dot{F}_\varepsilon(y^{(1)}) \\
 &\quad + \frac{25}{336}\Delta t^2 \dot{F}_\varepsilon(y^{(2)}),
 \end{aligned}$$

will have a final time error of  $E = O(\Delta t^5) + O(\varepsilon \Delta t)$ . For this fifth order method we require  $\varepsilon \ll \Delta t^4$  to obtain high order convergence, and once  $\Delta t$  is small enough we expect to see the first order convergence.

Figure 1 (right) shows that the linear stability region of this method is larger than that of the third and fourth order methods. Figure 4 shows that the stability of the method is very sensitive to the perturbation error  $\varepsilon$ .

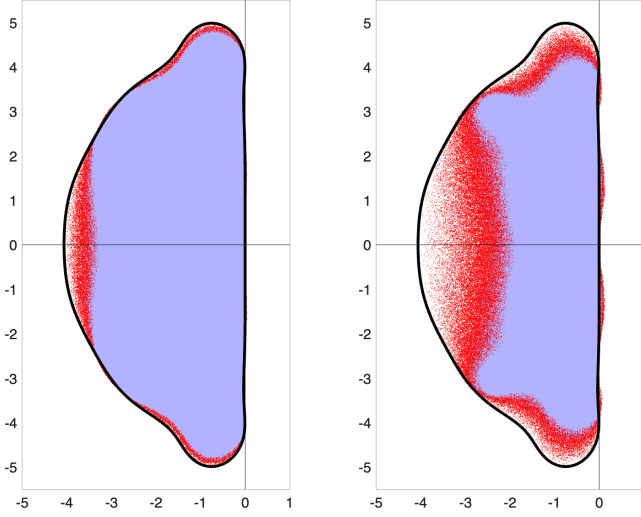


FIGURE 5. Perturbed Linear stability regions for the sixth order MP-TDRK method (5.7) with  $\varepsilon = 0.1$  (left) and  $\varepsilon = 0.5$  (right);

**5.4. Sixth Order Method.** For the sixth order method we use Tsai's methods from [6].

**TDRK method TDRK4s6p1e:** The four-stage sixth order method

$$\begin{aligned}
 y^{(1)} &= u^n + \frac{1}{4}\Delta t F(u^n) + \frac{1}{32}\Delta t^2 \dot{F}_\varepsilon(u^n) \\
 y^{(2)} &= u^n + \frac{2}{3}\Delta t F(u^n) - \frac{2}{81}\Delta t^2 \dot{F}_\varepsilon(u^n) + \frac{20}{81}\Delta t^2 \dot{F}_\varepsilon(y^{(1)}) \\
 y^{(3)} &= u^n + \Delta t F(u^n) + \frac{5}{4}\Delta t^2 \dot{F}_\varepsilon(u^n) \\
 &\quad - \frac{6}{5}\Delta t^2 \dot{F}_\varepsilon(y^{(1)}) + \frac{9}{20}\Delta t^2 \dot{F}_\varepsilon(y^{(2)}) \\
 (5.7) \quad u^{n+1} &= u^n + \Delta t F(u^n) + \frac{3}{40}\Delta t^2 \dot{F}_\varepsilon(u^n) + \frac{64}{225}\Delta t^2 \dot{F}_\varepsilon(y^{(1)}) \\
 &\quad + \frac{27}{200}\Delta t^2 \dot{F}_\varepsilon(y^{(2)}) + \frac{1}{180}\Delta t^2 \dot{F}_\varepsilon(y^{(3)}).
 \end{aligned}$$

This method will have a final time error of

$$E = O(\Delta t^6) + O(\varepsilon \Delta t),$$

so we expect to see high order when  $\varepsilon \ll \Delta t^5$ , but when  $\Delta t$  is larger we will see linear convergence.

Figure 1 (right) shows that the linear stability region of this method is larger than that all other methods, which may help offset the increased computational cost from this four stage method. However, Figure 5 shows that this method has a stability region that is extremely sensitive to the size of perturbation error  $\varepsilon$ .

## 6. NUMERICAL SIMULATIONS

The focus of this work is the numerical analysis framework described in Section 4 for developing and analyzing mixed precision TDRK methods. The methods studied as well as the new methods designed in Section 5 are meant to demonstrate that the perturbation order conditions developed in Section 4 accurately predict the convergence behavior. These methods are not optimized in any sense, including efficiency.

The simulations in this section confirm that the impact of the low precision perturbations on the accuracy of the solution is as expected from their design, and that larger perturbations require smaller time-steps for stability, as predicted by the perturbed stability regions in Figures 2, 3, 4, and 5. While the use of mixed precision has the potential for computational time-savings, in practice the efficiency of any given methods will depend on its design relative to the particular application and the relative costs of the operators  $F$  and  $\dot{F}$ . For these reasons we focus our numerical studies on the accuracy and stability of the methods, omitting any analysis of their efficiency.

**6.1. Linear advection with mixed precision.** We consider the linear advection equation

$$U_t + aU_x = 0$$

with  $a = 1$ , and  $x \in [-1, 1]$ . We use the initial condition  $U_0(x) = \sin(\pi x)$ , so that the solution is a sine wave at all times, and if we use Fourier spectral methods we have no error from the spatial discretization, so we observe only the time-discretization error. We implement the spatial discretization by defining the Fourier differentiation matrix  $\mathbf{D}_x$  with  $N_x$  points in space.

We discretize in space to obtain the system of ODEs

$$u_t = -a\mathbf{D}_x u.$$

We now use the three different third order mixed-precision TDRK methods (5.1), (5.2), and (5.3), to evolve the solution forward to final time  $T_f = 0.5$ .

Tables 1, 2, and 3 show the final time maximum norm errors compared to the exact solution  $U(x, t) = \sin(\pi(x - at))$  for  $N_x = 25, 50, 100$ , for each of the methods (5.1), (5.2), and (5.3), respectively. These results confirm that the methods display the perturbation order as predicted by the theory. This results in smaller errors from the mixed precision implementation of the methods with perturbation errors  $\epsilon\Delta t^m$  as  $m$  increases. It is notable that while for  $N_x = 25$  the mixed precision method converges for all values of  $\Delta t$ , as  $N_x$  gets larger we require smaller values of  $\Delta t$  for convergence. This effect is more pronounced as we move to lower precision. The mixed method inherits the stability properties of the low-precision method, so that while mixed precision improves the magnitude of the errors, it does not improve the value of  $\Delta t$  needed for stability of the method. However, the mixed precision method ensures that the method will converge as  $\Delta t$  continues to get much smaller, which is not the case for the lower precision method.

TABLE 1. Errors for mixed precision TDRK2s3p1e

$N_x$	$\Delta t$	64/64	64/32	32/32	64/16	16/16
25	$10^{-1}$	$2.04 \times 10^{-3}$	$1.88 \times 10^{-2}$	$1.86 \times 10^{-2}$	$4.83 \times 10^1$	$7.39 \times 10^1$
	$5 \times 10^{-2}$	$2.54 \times 10^{-4}$	$2.54 \times 10^{-4}$	$2.55 \times 10^{-4}$	$1.11 \times 10^{-2}$	$3.30 \times 10^{-2}$
	$2.5 \times 10^{-2}$	$3.17 \times 10^{-5}$	$3.18 \times 10^{-5}$	$3.36 \times 10^{-5}$	$6.33 \times 10^{-3}$	$2.91 \times 10^{-2}$
	$10^{-2}$	$2.03 \times 10^{-6}$	$2.15 \times 10^{-6}$	$4.25 \times 10^{-6}$	$2.60 \times 10^{-3}$	$2.91 \times 10^{-2}$
	$10^{-3}$	$2.03 \times 10^{-9}$	$2.37 \times 10^{-8}$	$3.37 \times 10^{-6}$	$2.82 \times 10^{-4}$	$4.33 \times 10^{-2}$
	$10^{-4}$	$2.03 \times 10^{-12}$	$2.56 \times 10^{-9}$	$1.17 \times 10^{-4}$	$2.85 \times 10^{-5}$	$3.86 \times 10^{-1}$
50	$10^{-1}$	$2.24 \times 10^{-3}$	$2.93 \times 10^5$	$3.18 \times 10^5$	N/A	N/A
	$5 \times 10^{-2}$	$2.60 \times 10^{-4}$	$1.08 \times 10^4$	$1.22 \times 10^4$	N/A	N/A
	$2.5 \times 10^{-2}$	$3.17 \times 10^{-5}$	$3.25 \times 10^{-5}$	$4.03 \times 10^{-5}$	$1.63 \times 10^{-2}$	$6.69 \times 10^{-2}$
	$10^{-2}$	$2.03 \times 10^{-6}$	$2.98 \times 10^{-6}$	$1.24 \times 10^{-5}$	$1.05 \times 10^{-2}$	$8.25 \times 10^{-2}$
	$10^{-3}$	$2.03 \times 10^{-9}$	$1.14 \times 10^{-7}$	$9.86 \times 10^{-6}$	$8.45 \times 10^{-4}$	$9.30 \times 10^{-2}$
	$10^{-4}$	$2.03 \times 10^{-12}$	$1.18 \times 10^{-8}$	$1.48 \times 10^{-4}$	$8.56 \times 10^{-5}$	$3.87 \times 10^{-1}$
100	$10^{-1}$	$3.13 \times 10^3$	$1.25 \times 10^{12}$	$1.25 \times 10^{12}$	N/A	N/A
	$5 \times 10^{-2}$	$2.63 \times 10^9$	$9.83 \times 10^{17}$	$9.90 \times 10^{17}$	N/A	N/A
	$2.5 \times 10^{-2}$	$1.99 \times 10^7$	$6.24 \times 10^{15}$	$6.74 \times 10^{15}$	N/A	N/A
	$10^{-2}$	$2.03 \times 10^{-6}$	$8.68 \times 10^{-6}$	$1.81 \times 10^{-5}$	$8.05 \times 10^{-2}$	$1.53 \times 10^{-1}$
	$10^{-3}$	$2.03 \times 10^{-9}$	$6.01 \times 10^{-7}$	$1.31 \times 10^{-5}$	$7.45 \times 10^{-3}$	$1.57 \times 10^{-1}$
	$10^{-4}$	$2.06 \times 10^{-12}$	$6.15 \times 10^{-8}$	$1.53 \times 10^{-4}$	$7.37 \times 10^{-4}$	$2.02 \times 10^{-1}$

TABLE 2. Errors for mixed precision TDRK2s3p2e

$N_x$	$\Delta t$	64/64	64/32	32/32	64/16	16/16
25	$10^{-1}$	$2.03 \times 10^{-3}$	$5.42 \times 10^{-3}$	$4.74 \times 10^{-3}$	$1.07 \times 10^1$	$1.18 \times 10^1$
	$5 \times 10^{-2}$	$2.54 \times 10^{-4}$	$2.54 \times 10^{-4}$	$2.52 \times 10^{-4}$	$4.63 \times 10^{-3}$	$3.35 \times 10^{-2}$
	$2.5 \times 10^{-2}$	$3.16 \times 10^{-5}$	$3.17 \times 10^{-5}$	$3.15 \times 10^{-5}$	$9.44 \times 10^{-4}$	$2.84 \times 10^{-2}$
	$10^{-2}$	$2.03 \times 10^{-6}$	$2.04 \times 10^{-6}$	$3.55 \times 10^{-6}$	$1.54 \times 10^{-4}$	$3.13 \times 10^{-2}$
	$10^{-3}$	$2.03 \times 10^{-9}$	$2.15 \times 10^{-9}$	$3.21 \times 10^{-6}$	$1.58 \times 10^{-6}$	$8.20 \times 10^{-2}$
	$10^{-4}$	$2.03 \times 10^{-12}$	$3.40 \times 10^{-12}$	$8.77 \times 10^{-6}$	$1.58 \times 10^{-8}$	$6.26 \times 10^{-1}$
50	$10^{-1}$	$2.03 \times 10^{-3}$	$7.47 \times 10^2$	$7.04 \times 10^2$	N/A	N/A
	$5 \times 10^{-2}$	$2.54 \times 10^{-4}$	$2.73 \times 10^2$	$2.74 \times 10^2$	N/A	N/A
	$2.5 \times 10^{-2}$	$3.16 \times 10^{-5}$	$3.28 \times 10^{-5}$	$3.51 \times 10^{-5}$	$7.54 \times 10^{-3}$	$7.13 \times 10^{-2}$
	$10^{-2}$	$2.03 \times 10^{-6}$	$2.17 \times 10^{-6}$	$9.83 \times 10^{-6}$	$1.56 \times 10^{-3}$	$7.71 \times 10^{-2}$
	$10^{-3}$	$2.03 \times 10^{-9}$	$3.85 \times 10^{-9}$	$9.56 \times 10^{-6}$	$1.68 \times 10^{-5}$	$9.46 \times 10^{-2}$
	$10^{-4}$	$2.03 \times 10^{-12}$	$2.00 \times 10^{-11}$	$1.23 \times 10^{-5}$	$1.72 \times 10^{-7}$	$5.66 \times 10^{-1}$
100	$10^{-1}$	$1.36 \times 10^{-1}$	$5.95 \times 10^7$	$6.01 \times 10^7$	N/A	N/A
	$5 \times 10^{-2}$	$5.36 \times 10^3$	$2.58 \times 10^{12}$	$2.55 \times 10^{12}$	N/A	N/A
	$2.5 \times 10^{-2}$	$3.27 \times 10^3$	$1.40 \times 10^{12}$	$1.55 \times 10^{12}$	N/A	N/A
	$10^{-2}$	$2.03 \times 10^{-6}$	$2.92 \times 10^{-6}$	$1.34 \times 10^{-5}$	$9.32 \times 10^{-3}$	$9.76 \times 10^{-2}$
	$10^{-3}$	$2.03 \times 10^{-9}$	$1.74 \times 10^{-8}$	$1.35 \times 10^{-5}$	$1.47 \times 10^{-4}$	$1.06 \times 10^{-1}$
	$10^{-4}$	$2.05 \times 10^{-12}$	$1.62 \times 10^{-10}$	$1.35 \times 10^{-5}$	$1.48 \times 10^{-6}$	$4.19 \times 10^{-1}$

This behavior explained by the stability regions plotted in Figure 2. Two factors are at play here. First, as the perturbation grows larger (i.e. the precision is lower), the linear stability region shrinks. In addition, the value of  $\varepsilon$  is not only related to the precision, but also to the size of the problem, as we explained in Remark 4.1. For this reason, even for the same precision,  $\varepsilon$  is larger as  $N_x$  is larger, resulting in smaller stability regions.

TABLE 3. Errors for mixed precision TDRK3s3p

$N_x$	$\Delta t$	64/64	64/32	32/32	64/16	16/16
25	$10^{-1}$	$6.95 \times 10^{-4}$	$2.69 \times 10^{-3}$	$2.13 \times 10^{-3}$	$1.10 \times 10^{-1}$	$3.37 \times 10^0$
	$5 \times 10^{-2}$	$8.51 \times 10^{-5}$	$8.53 \times 10^{-5}$	$8.61 \times 10^{-5}$	$1.68 \times 10^{-3}$	$2.82 \times 10^{-2}$
	$2.5 \times 10^{-2}$	$1.06 \times 10^{-5}$	$1.06 \times 10^{-5}$	$1.24 \times 10^{-5}$	$2.69 \times 10^{-4}$	$2.91 \times 10^{-2}$
	$10^{-2}$	$6.76 \times 10^{-7}$	$6.76 \times 10^{-7}$	$3.25 \times 10^{-6}$	$1.81 \times 10^{-5}$	$3.08 \times 10^{-2}$
	$10^{-3}$	$6.76 \times 10^{-10}$	$6.76 \times 10^{-10}$	$3.40 \times 10^{-6}$	$1.81 \times 10^{-8}$	$3.74 \times 10^{-2}$
	$10^{-4}$	$6.76 \times 10^{-13}$	$6.77 \times 10^{-13}$	$1.01 \times 10^{-5}$	$1.80 \times 10^{-11}$	$3.98 \times 10^{-1}$
50	$10^{-1}$	$7.28 \times 10^{-4}$	$4.52 \times 10^4$	$4.28 \times 10^4$	N/A	N/A
	$5 \times 10^{-2}$	$8.52 \times 10^{-5}$	$1.47 \times 10^2$	$8.42 \times 10^1$	N/A	N/A
	$2.5 \times 10^{-2}$	$1.06 \times 10^{-5}$	$1.10 \times 10^{-5}$	$1.84 \times 10^{-5}$	$2.80 \times 10^{-3}$	$6.74 \times 10^{-2}$
	$10^{-2}$	$6.76 \times 10^{-7}$	$7.15 \times 10^{-7}$	$1.05 \times 10^{-5}$	$2.83 \times 10^{-4}$	$8.01 \times 10^{-2}$
	$10^{-3}$	$6.76 \times 10^{-10}$	$7.17 \times 10^{-10}$	$1.03 \times 10^{-5}$	$2.72 \times 10^{-7}$	$9.42 \times 10^{-2}$
	$10^{-4}$	$6.72 \times 10^{-13}$	$7.26 \times 10^{-13}$	$2.07 \times 10^{-5}$	$2.82 \times 10^{-10}$	$4.92 \times 10^{-1}$
100	$10^{-1}$	$3.81 \times 10^2$	$1.63 \times 10^{11}$	$1.54 \times 10^{11}$	N/A	N/A
	$5 \times 10^{-2}$	$3.18 \times 10^7$	$1.69 \times 10^{16}$	$1.59 \times 10^{16}$	N/A	N/A
	$2.5 \times 10^{-2}$	$1.15 \times 10^3$	$6.86 \times 10^{11}$	$3.87 \times 10^{11}$	N/A	N/A
	$10^{-2}$	$6.77 \times 10^{-7}$	$1.05 \times 10^{-6}$	$1.39 \times 10^{-5}$	$4.29 \times 10^{-3}$	$1.02 \times 10^{-1}$
	$10^{-3}$	$6.76 \times 10^{-10}$	$1.41 \times 10^{-9}$	$1.34 \times 10^{-5}$	$5.70 \times 10^{-6}$	$1.10 \times 10^{-1}$
	$10^{-4}$	$7.09 \times 10^{-13}$	$1.43 \times 10^{-12}$	$2.04 \times 10^{-5}$	$5.52 \times 10^{-9}$	$1.92 \times 10^{-1}$

Figure 6 shows the final time maximum-norm errors compared to the exact solution for  $U(x, t) = \sin(\pi(x - at))$  for  $N_x = 50$  with double/half mixed precision (left) and with double/single mixed precision (right). Note that as  $\Delta t$  gets very small, the low precision methods do not converge, and indeed the error grows. The mixed precision methods converge as  $\varepsilon \Delta t^m$  for  $m = 1, 2, 3$  for (5.1), (5.2), and (5.3), respectively. The top figures show double precision mixed with half precision, and the bottom figures show double precision mixed with single precision. We observe that for the mixed double/single method the errors from the  $m = 2$  method (5.2) look very close to those from the high precision method, and the error from the  $m = 3$  method (5.3) are indistinguishable from those from the high precision method.

The two sides of Figure 6 show the impact of different mixed precision implementation. On the left we have **Implementation 1**, in which we compute the second derivative matrix in low precision by using low precision FFTs. This is computationally faster but results in a buildup of the low precision rounding errors and a larger  $\varepsilon$ . This is the primary implementation we use in this work. On the right we show the result of a more accurate **Implementation 2**, in which we compute the second derivative matrix in high precision initially, and then downcast it to lower precision and use it in the computation of  $\dot{F}$ . We observe that the mixed precision error lines in **Implementation 2** are shifted downwards by one to two orders of magnitude compared to **Implementation 1**. This shows that the smaller  $\varepsilon$  results in significantly smaller errors.

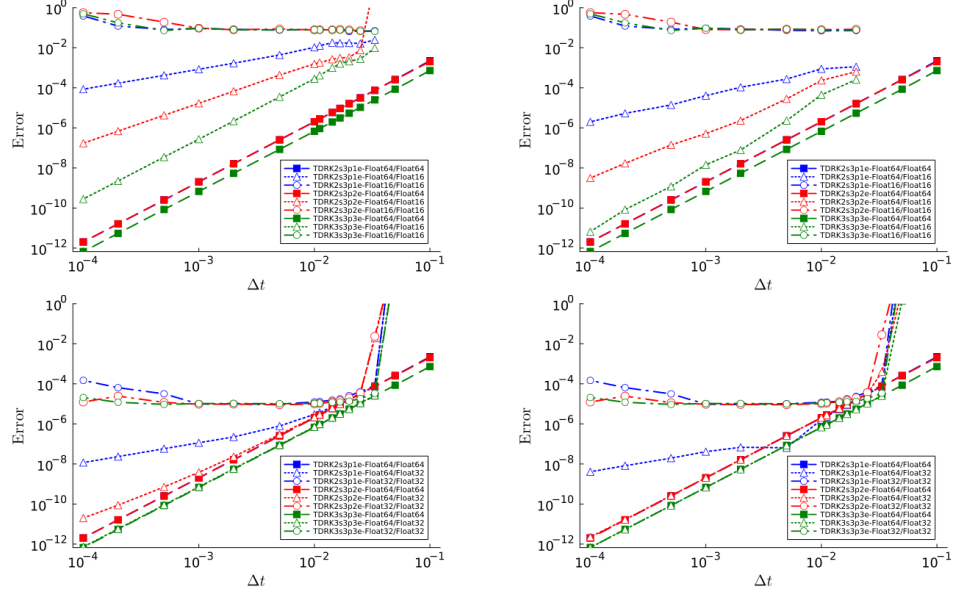


FIGURE 6. Mixed double/half precision third order methods applied to the linear advection equation for  $N_x = 50$ . On the left is **Implementation 1** and on the right is the more accurate but also more costly **Implementation 2**. Top: double/half; Bottom: double/single. Note that NaNs and INFs do not plot, so that the lines end at smaller  $\Delta t$ .

Figure 7 shows the error plots for  $N_x = 50$  for the two fourth order methods (5.4) and (5.5) that have perturbation orders  $O(\varepsilon \Delta t)$  and  $O(\varepsilon \Delta t^2)$ , respectively. On the left we see the behavior with double precision mixed with half precision, and on the right the double precision mixed with single precision. The errors are significantly lower in the double/single implementation, and we see a larger  $\Delta t$  is allowed for stability. We observe that,

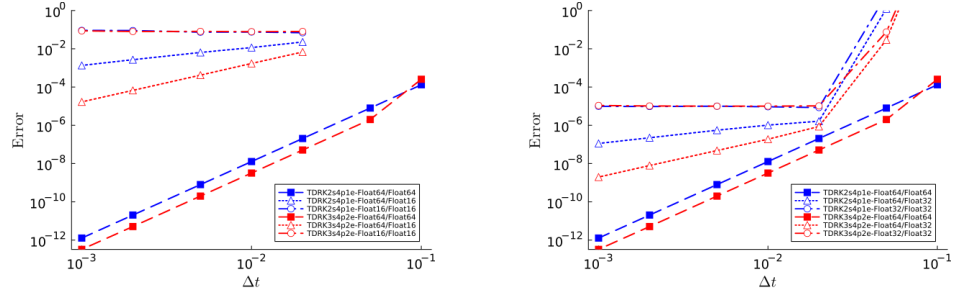


FIGURE 7. Mixed precision fourth order methods applied to the linear advection equation for  $N_x = 50$ . On the left is double/half and in the right is double/single.

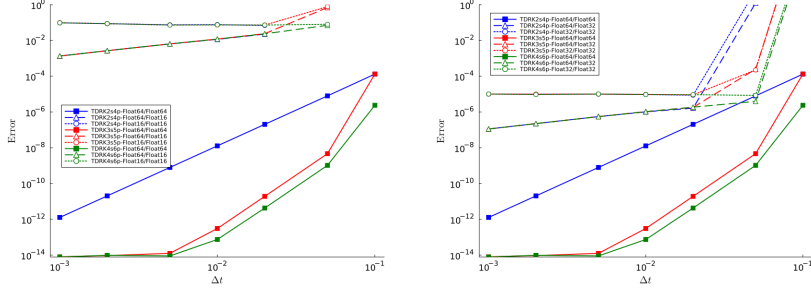


FIGURE 8. Mixed precision methods of order  $p = 4, 5, 6$  and perturbation order  $m = 1$  applied to the linear advection equation for  $N_x = 50$ . Left has mixed double/half precision and right has mixed double/single precision.

as predicted by the theory, the TDRK2s4p1e method (5.4) has first order convergence once  $\Delta t$  is small enough compared to  $\varepsilon$ , while the TDRK3s4p2e method (5.5) has second order convergence.

Figure 8 shows the error plots for  $N_x = 50$  for the the fourth, fifth, and sixth order mixed precision TDRK methods (5.4), (5.6), (5.7), that have perturbation errors  $O(\varepsilon\Delta t)$ . On the left we see the behavior with double precision mixed with half precision, and on the right the double precision mixed with single precision. These methods all converge linearly in the mixed precision setting. The figure confirms the design order accuracy of  $p = 4, 6$ . For  $p = 5$  we have higher order convergence than we expect. Closer analysis of the coefficients in (5.6) show that the order condition corresponding to the linear tree (the tall tree) is satisfied. This is due to the simplified structure inherent in Tsai's methods, which causes several of the sixth order trees to be satisfied, as well, due to the high stage order that is enforced in Tsai's methods. Thus, the  $p = 5$  method is in fact sixth order when applied to linear problems. We also observe first order convergence in the mixed precision methods, as expected, with the double/single errors four orders of magnitude smaller than the double/half errors.

**6.2. Inviscid Burgers' equation with Fourier spectral methods.** In this subsection we solve the inviscid Burgers' equation

$$(6.1) \quad U_t + \left( \frac{1}{2} U^2 \right)_x = 0,$$

for  $x \in [-1, 1]$ , with the initial condition  $U_0(x) = \frac{1}{2} + \frac{1}{4} \sin(\pi x)$ .

We discretize in space using the spectral differentiation matrix described above, to obtain

$$(6.2) \quad u_t = F(u) = -\mathbf{D}_x f(u)$$

and compute the second derivative

$$\dot{F}(u) = \mathbf{D}_x (u F(u)).$$

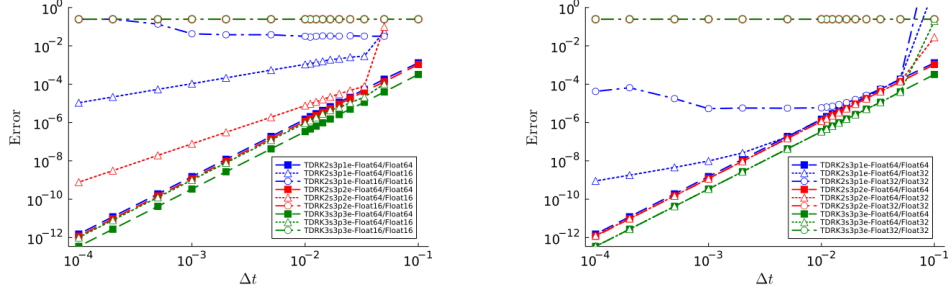


FIGURE 9. Mixed precision third order methods applied to Burger's equation for  $N_x = 50$ . On the left is double/half and in the right is double/single. Method (5.1) in blue, method (5.2) in red, and method (5.3) in green.

We evolve the solution forward in time to  $T_f = 0.5$  using the different mixed-precision TDRK methods. For each  $N_x$ , the reference solution is computed in quad precision using the Shu-Osher SSP33 method [29] with the same  $N_x$  and a refined time step of  $\Delta t = 10^{-7}$ .

Figure 9 shows the errors from Burgers' equation evolved with the third order methods (5.1), (5.2), and (5.3) for double/half (left) double/single (right). This figure shows the impact of the perturbation order  $\varepsilon \Delta t^m$  with increasing  $m$ . Notably, for both precisions, the errors from the  $O(\varepsilon \Delta t^3)$  mixed precision method (5.3) are indistinguishable from the full precision implementation. For double/single, the errors from the  $O(\varepsilon \Delta t^2)$  mixed precision method (5.2) are also indistinguishable from the full precision implementation, and the errors from the  $O(\varepsilon \Delta t)$  mixed precision method (5.1) converge at third order until below  $\Delta t < 10^{-2}$ , and then they switch to first order, as the perturbation error dominates.

Figure 10 shows the errors from Burgers' equation evolved with the fourth order methods (5.4) in blue and (5.5) in red. As expected, the methods are

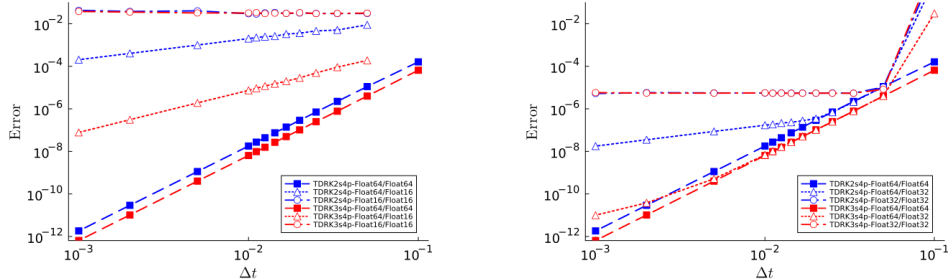


FIGURE 10. Errors from Burger's equation for  $N_x = 50$  evolved with the mixed precision fourth order methods (5.4) and (5.5). On the left is double/half and in the right is double/single.

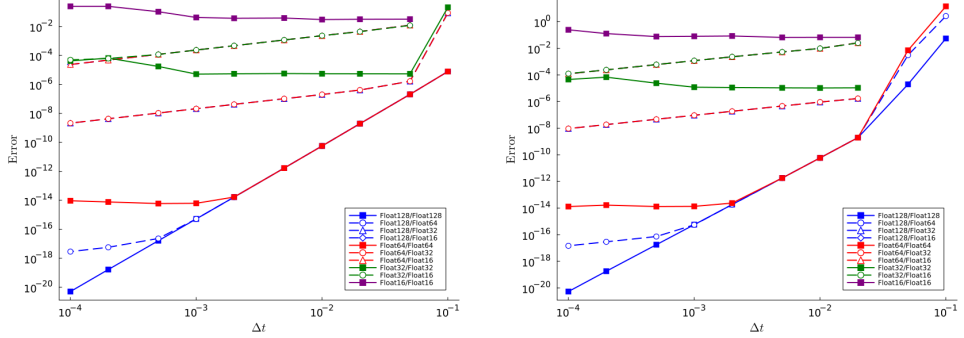


FIGURE 11. Mixed precision fifth order method TDRK3s5p1e (5.5) applied to Burgers' equation for (left)  $N_x = 50$ , and (right)  $N_x = 100$ .

fourth order in full precision, first order in mixed precision, and not convergent in low precision. While in mixed double/half precision (left) there is a difference of over four orders of magnitude between the mixed precision and full precision implementation of method (5.5) (in red), in mixed double/single precision (right) the errors from method (5.5) are fifth order until well below  $10^{-2}$ , at which point they switch over to second order. This is a clear illustration of the errors  $E = O(\Delta t^4) + O(\varepsilon \Delta t^2)$ , where the fourth order error dominates until  $\Delta t$  becomes small enough compared to  $\varepsilon$  that the second order error becomes dominant.

Figures 11 and 12 show the errors from the mixed precision fifth order (5.6) and sixth order (5.7) methods (respectively) on the inviscid Burgers' equation above with  $N_x = 50$  points (left) and  $N_x = 100$  points (right). These figures show mixed precision simulations with precisions from quad precision (Float128) to half precision (Float16). For both the fifth order method in Figure 11 and the sixth order method in Figure 12 we see that

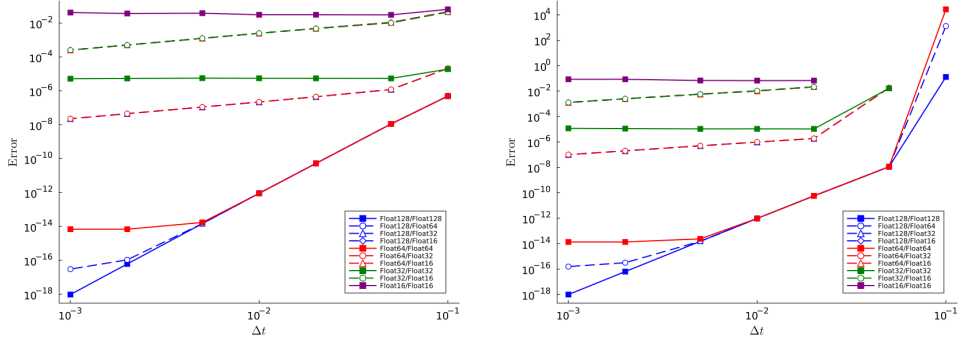


FIGURE 12. The mixed precision sixth order TDRK4s6p method (5.7) applied to Burgers' equation for (left)  $N_x = 50$ , and (right)  $N_x = 100$ .

larger  $N_x$  and lower precision result in a smaller  $\Delta t$  required for stability. For fifth order, the  $N_x = 50$  plots (left) are stable for double precision, quad precision, and mixed quad/double computation. For the mixed double/single and quad/single, the errors are high, for the largest  $\Delta t$  tested, which suggests incipient instability. For the half precision as well as the mixed double/half and single/half the methods are clearly not stable for the largest  $\Delta t$  tested. The case for  $N_x = 100$  is clearer, as the methods that are below double precision are all unstable for the largest two values of  $\Delta t$ . In all cases, the mixed quad/double codes show fifth order convergence until  $\Delta t$  is small enough, at which point the perturbation error of order one becomes visible. The value of  $\Delta t$  for which this happens is smaller for  $N_x = 50$  than for  $N_x = 100$ , which is expected since the value of  $\varepsilon$  will depend not only on the precision but on the size of the matrix  $\mathbf{D}_x$  as well.

For sixth order, the  $N_x = 50$  plots (left) are all stable, while the  $N_x = 100$  plots (right) are stable for all  $\Delta t$  for the double precision, quad precision, and mixed quad/double computation. A smaller  $\Delta t$  is needed for stability for single precision and mixed quad/single and double/single. An even smaller  $\Delta t$  is needed for stability for half precision, mixed single/half, and double/half. As in the fifth order plots in Figure 11, we see that the mixed quad/double codes show sixth order convergence until  $\Delta t$  is small enough, at which point the perturbation error of order one becomes visible. As expected, the value of  $\Delta t$  for which this happens is smaller for  $N_x = 50$  than for  $N_x = 100$ .

## 7. CONCLUSIONS

In this work we extended Grant's additive framework for mixed accuracy and mixed precision Runge–Kutta methods [12] to mixed precision two-derivative methods. This enables us to naturally adopt a mixed precision computation of the second derivative into existing  $p = 3, 4, 5, 6$ th order methods (5.1), (5.4), (5.6), and (5.7) (respectively), and show using the perturbed order conditions that we expect a global order of  $O(\Delta t^p) + O(\varepsilon \Delta t)$ . This framework further allowed us to develop third order methods that have higher order perturbation errors, the TDRK2s3p2e method (5.2) with global order of  $O(\Delta t^3) + O(\varepsilon \Delta t^2)$ , and the TDRK3s3p3e method (5.3) with global order of  $O(\Delta t^3) + O(\varepsilon \Delta t^3)$ , and a fourth order TDRK3s4p2e method (5.5) with global order of  $O(\Delta t^4) + O(\varepsilon \Delta t^2)$ . The numerical simulations in Section 6 confirm that the methods perform as expected in the time-evolution of linear and nonlinear PDEs.

The mixed accuracy framework we presented in Section 4 can be generalized to mixed precision computations of  $F$  as well as  $\dot{F}$ . It can be extended to higher order and adapted to perturbations that are smooth, or to higher orders in  $\varepsilon$  as well as  $\Delta t$ . Wherever two-derivative Runge–Kutta methods are used, this approach can be modified and extended to allow for significant computational savings. Future directions for this approach include

these extensions, as well as a formulation of this framework for general linear methods (GLMs). Further developments will be application dependent, in order to optimize for efficiency. For example, depending on the trade-off between the computational cost of the full precision operators and the lower precision operators, it may be worthwhile to produce higher order methods that will use different balance of full precision and reduced precision computations. These methods may be optimized for other properties including linear stability regions or strong stability properties. Now that the perturbation order conditions are determined, mixed precision two-derivative Runge–Kutta methods can be tailored and optimized as needed for different problems, as determined by the computational cost of each component.

#### AUTHOR CONTRIBUTION STATEMENT

**Sigal Gottlieb** was responsible for conceptualization of this project. SG was responsible for developing the new fourth order methods in Section 5.2, and was primarily responsible for choosing the problems and methods in Section 6, and in writing the results in that section. SG wrote the first draft of this manuscript, and was responsible for the final edits.

**Zachary J. Grant** was responsible for developing the perturbation order conditions, and for developing the new third order methods in Section 5.1. ZJG modified LeVeque’s stability region codes to produce all the plots in Section 5. ZJG co-wrote Sections 2 and 3, carefully proofread the entire paper, and made numerous editorial suggestions to improve the presentation.

**Cesar Herrera** was responsible for all the codes, computations, and preparation of graphs and tables in Section 6, was involved in discussions on the presentation of the material. CH provided the expertise on mixed precision implementation in julia language, and all the numerical results. He read, commented, and edited the entire manuscript.

#### REFERENCES

- [1] R. P. K. Chan A. Y. J. Tsai and S. Wang. Two-derivative Runge–Kutta methods for PDEs using a novel discretization approach. *Numerical Algorithms*, 65:687–703, 2014.
- [2] Cody J. Balos, Steven Roberts, and David J. Gardner. Leveraging mixed precision in exponential time integration methods. In *2023 IEEE High Performance Extreme Computing Conference (HPEC)*, pages 1–8, 2023.
- [3] Sigal Gottlieb Ben Burnett and Zachary J. Grant. Stability analysis and performance evaluation of additive mixed-precision runge-kutta methods.
- [4] Ben Burnett, Sigal Gottlieb, Zachary J. Grant, and Alfa Heryudono. Performance evaluation of mixed-precision runge-kutta methods. In *2021 IEEE High Performance Extreme Computing Conference (HPEC)*, pages 1–6, 2021.
- [5] Erin Carson, Nicholas J. Higham, and Srikara Pranesh. Three-precision gmres-based iterative refinement for least squares problems. *SIAM Journal on Scientific Computing*, 42(6):A4063–A4083, 2020.
- [6] R. P. K. Chan and A. Y. J. Tsai. On explicit two-derivative Runge–Kutta methods. *Numerical Algorithms*, 53:171–194, 2010.

- [7] A.J. Christlieb, S. Gottlieb, Z. Grant, and D. C. Seal. Explicit strong stability preserving multistage two-derivative time-stepping schemes. *Journal of Scientific Computing*, 68(3):914–942, 2016.
- [8] Matteo Croci and Giacomo Rosilho de Souza. Mixed-precision explicit stabilized runge–kutta methods for single- and multi-scale differential equations. *Journal of Computational Physics*, 464:111349, 2022.
- [9] Y. Guclu D. C. Seal and A. J. Christlieb. High-order multiderivative time integrators for hyperbolic conservation laws. *Journal of Scientific Computing*, 60:101–140, 2014.
- [10] Z. Du and J. Li. A hermite weno reconstruction for fourth order temporal accurate schemes based on the grp solver for hyperbolic conservation laws. *Journal of Computational Physics*, 355:385–396, 2018.
- [11] Z. Grant, S. Gottlieb, and D.C. Seal. A strong stability preserving analysis for explicit multistage two-derivative time-stepping schemes based on taylor series conditions. *Communications on Applied Mathematics and Computation*, 1:21–59, 2019.
- [12] Zachary J. Grant. Perturbed runge-kutta methods for mixed precision applications. *Journal of Scientific Computing*, 92(1):1–20, 2022.
- [13] Marcel Koch Ivo Dravins and Katharina Kormann. Performance evaluation of mixed-precision runge–kutta methods for the solution of partial differential equations. *The International Journal of High Performance Computing Applications*, 2025.
- [14] Zachary J. Grant Cesar Herrera Tej Sai Kakumanu Michael H. Sawicki Monica Stephens John Driscoll, Sigal Gottlieb. Stable corrections for perturbed diagonally implicit runge–kutta methods. *Manuscript in Preparation*.
- [15] K. Kastlunger and G. Wanner. On Turan type implicit Runge-Kutta methods. *Computing (Arch. Elektron. Rechnen)*, 9:317–325, 1972.
- [16] K. H. Kastlunger and G. Wanner. Runge Kutta processes with multiple nodes. *Computing (Arch. Elektron. Rechnen)*, 9:9–24, 1972.
- [17] Carl Kelley. Newton’s method in mixed precision. *SIAM Review*, 64:191–211, 02 2022.
- [18] J. Li and Z. Du. A two-stage fourth order time-accurate discretization for lax-wendroff type flow solvers i. hyperbolic conservation laws. *SIAM J. Sci. Computing*, 38:3046–3069, 2016.
- [19] E. Squintana-Ort M. Petschow and P. Bientinesi. Improved accuracy and parallelism for mrrr-based eigensolvers – a mixed precision approach. *SIAM Journal on Scientific Computing*, 36(2):C240–C263, 2014.
- [20] Marc Marot-Lassauzaie and Michael Bader. Mixed-precision in high-order methods: the impact of floating-point precision on the ader-dg algorithm, 2025.
- [21] Craig Lucas Françoise Tisseur Mawussi Zounon, Nicholas J. Higham. Performance impact of precision reduction in sparse linear systems solvers. *J Comput. Sci.*, 8:e778, 2022.
- [22] T. Mitsui. Runge-Kutta type integration formulas including the evaluation of the second derivative. i. *Publ. Res. Inst. Math. Sci.*
- [23] Arsène Marzorati Mouhamad Al Sayed Ali, Samuel Bernard and Jonathan Rouzaud-Cornabas. Mixed precision implicit numerical schemes for systems of ordinary differential equations. *Numerical Algorithms*, 2025.
- [24] H. Ono and T. Yoshida. Two-stage explicit Runge-Kutta type methods using derivatives. *Japan J. Indust. Appl. Math.*, 21:61–374, 2004.
- [25] L. Pan, K. Xu, Q. Li, and J. Li. An efficient and accurate two-stage fourth-order gas-kinetic scheme for the euler and navier–stokes equations. *Journal of Computational Physics*.
- [26] Zachary J. Grant Leah F. Isherwood Gaurav Khanna Scott E. Field, S. Gottlieb. A gpu-accelerated mixed-precision weno method for extremal black hole and gravitational wave physics computations. *Commun. Appl. Math. Comput.*, 5:97–115, 2023.
- [27] H. Shintani. On one-step methods utilizing the second derivative. *Hiroshima Mathematical Journal*.

- [28] H. Shintani. On explicit one-step methods utilizing the second derivative. *Hiroshima Mathematical Journal*, 2:353–368, 1972.
- [29] C.-W. Shu. Total-variation diminishing time discretizations. *SIAM Journal on Scientific Statistical Computing*, 9:1073–1084, 1988.
- [30] D. D. Stancu and A. H. Stroud. Quadrature formulas with simple Gaussian nodes and multiple fixed nodes. *Math. Comp.*, 17:384–394, 1963.
- [31] P. Turán. On the theory of the mechanical quadrature. *Acta Sci. Math. Szeged*, 12:30–37, 1950.

*Email address*, Sigal Gottlieb: [sgottlieb@umassd.edu](mailto:sgottlieb@umassd.edu)

*Email address*, Zachary J. Grant: [zgrant@umassd.edu](mailto:zgrant@umassd.edu)

*Email address*, César Herrera: [herre125@purdue.edu](mailto:herre125@purdue.edu)

(Sigal Gottlieb & Zachary J. Grant) MATHEMATICS DEPARTMENT, UNIVERSITY OF MASSACHUSETTS DARTMOUTH, NORTH DARTMOUTH, MA 02747.

(César Herrera) DEPARTMENT OF MATHEMATICS, PURDUE UNIVERSITY, 150 NORTH UNIVERSITY STREET. WEST LAFAYETTE, INDIANA 47907-2067